npj | complexity

Article

Article in Press

https://doi.org/10.1038/s44260-026-00098-8

Spectra of random graphs with discrete scale invariance

Check for updates

Alessio Catanzaro[1,2,3,5] ✉, Rajat Subhra Hazra[4,5] & Diego Garlaschelli[1,2,5]

Random graphs defined by an occurrence probability invariant under node aggregation have been identified recently in the context of network renormalization. The invariance property requires to draw edges with a specific probability that, in the annealed case, depends on a necessarily infinite-mean node fitness. The diverging mean determines many properties that are uncommon in models with independent edges, but at the same time widespread in real-world networks. Here, we focus on the leading eigenvalues and eigenvectors of the adjacency matrix of the model, where the n nodes are assigned a Pareto(a)-distributed fitness with $0 < a < 1$. We find that the leading eigenvalues are of order $\sqrt{n}$, alternate in sign and are located at the intersection between the real axis and a logarithmic spiral in the complex plane, which we characterize analytically in terms of the Gamma function. We also calculate the associated eigenvectors, finding complex-valued scaling exponents and log-periodicity, which are signatures of discrete scale-invariance. In contrast with typical finite-rank behaviour of random graphs, we find that a growing number of the leading eigenvalues emerges from the bulk, whose edge extends up to order $\sqrt{n}$ and therefore reaches the same scale as that of the structural eigenvalues.

Many models have been proposed to reproduce the heterogeneous structure ubiquitously observed in real-world networks. Among these, a wide class of random graph models assigns a weight (or fitness, or hidden variable) x_i to each vertex i ($i = 1, n$ where n is the number of nodes) from a usually fat-tailed distribution $\rho(x)$, and connects pairs of vertices i and j with a probability p_{ij} that is a certain positive function $f(x_i, x_j)$[1–4].

Recently, in the context of network renormalization[5,6], a specific such model that complements the heterogeneity of nodes with an invariance principle under graph coarse-graining has been identified[7–11]. In this so-called (annealed) multi-scale model (MSM), one may group nodes into equally sized 'supernodes', each inheriting the sum of the fitness of its members, and impose that both the connection probability $p_{ij} = f(x_i, x_j)$ and the fitness distribution $\rho(x)$ remain unchanged in their functional form, while their parameters follow exact renormalization rules. In other words, aggregating nodes into supernodes according to any homogeneous partition —and connecting two supernodes whenever there is a connection between any of their constituent nodes—defines a coarse-grained version of the graph, governed by an occurrence probability that has the same functional form as that of the original graph, up to a rescaling of the parameters[7,9].

This renormalization scheme does not rely on any underlying geometry or distance notion between nodes. This stands in contrast to geometric renormalization approaches[12,13], where the nodes to be merged need to be spatially proximate, and a preliminary definition of metric distance is needed. Rather, when nodes are merged into supernodes of equal cardinality, the invariance requirement in the MSM is closer in spirit to the concept of discrete scale invariance[14], whose consequences for the graph properties have not been investigated so far and are one of our main focuses here.

In particular, we are interested in the spectral properties[15] of the MSM, which turn out to be quite unique due to the peculiar structure of the fitness. Indeed, the requirement that the node fitness is a positive random ('annealed') variable that is stable under addition implies that it has an α-stable distribution with infinite mean ($0 < \alpha < 1$)[7,9], where classical random matrix results[15–21] break down. When a symmetric random matrix is decomposed into a low-rank informative part plus noise, strong signals can produce eigenvalue outliers outside the bulk spectrum, as first shown in ref. 22. In networks, such outliers reveal structures like communities or hubs[15,23]. While infinite-mean regimes have been studied for Lévy matrices[24–26], random graphs add further randomness from adjacency realizations, not captured by those approaches. Our goal is to shed light on the surprising behaviour of the eigenmodes of the adjacency matrix in this infinite-mean regime, which follows from discrete node aggregation

[1]Network Unit, IMT Lucca, Lucca, Italy. [2]Lorentz Institute for Theoretical Physics, Leiden University, Leiden, The Netherlands. [3]Dipartimento di Fisica, Universitá di Palermo, Palermo, Italy. [4]Mathematical Institute, Leiden University, Leiden, The Netherlands. [5]These authors contributed equally: Alessio Catanzaro, Rajat Subhra Hazra, Diego Garlaschelli. ✉e-mail: alessio.catanzaro@imtlucca.it

invariance. From a network-science perspective, the leading eigenvalues and eigenvectors are useful because they describe the large-scale structure created by the node fitnesses. In an actual graph realization this structure is mixed with the randomness of the edge variables. The leading spectral modes help identify which part of the spectrum reflects the multi-scale organization of the model, and which part belongs to the random bulk. In standard finite-mean hidden-variable models, only finitely many such structural modes are usually expected to stand out. In the MSM, by contrast, the number of visible modes grows slowly with the system size. This makes the leading spectrum a possible signature of discrete scale invariance and of the log-periodic behaviour generated by repeated coarse-graining. More generally, our analysis suggests a way to study random graph spectra in models where the expected adjacency matrix is not finite-rank, but still has only a slowly growing number of relevant modes.

Results

Model definition and matrix decomposition

The annealed MSM is an inhomogeneous random graph on n nodes, each node i being assigned a positive weight x_i, sampled independently from an α-stable distribution $\rho_\alpha(x)$, hence with power-law tails decaying as $x^{-1-\alpha}$ for $0<\alpha<1$ [7]. In this regime of α, every moment of $\rho_\alpha(x)$ diverges. Given x_i and x_j, the probability that an edge exists between i and j is

$$p_{ij} = f_n(x_i, x_j) = 1 - \exp(-\varepsilon_n x_i x_j), \quad i,j = 1,n \tag{1}$$

if $i \neq j$ and $p_{ii} = 0$ if $i = j$, where the parameter ε_n may be chosen to scale with n in a desired way. The exponential form in Eq. (1) is used due to its compatibility with the MSM coarse-graining rule. Indeed, if I and J are two supernodes with aggregated fitnesses

$$X_I = \sum_{i\in I} x_i, \qquad X_J = \sum_{j\in J} x_j$$

(where $i \in I$ denotes that node i belongs to the supernode I), and if two supernodes are connected whenever at least one microscopic edge between them is present, then

$$1 - \prod_{i\in I, j\in J}(1-p_{ij}) = 1 - \exp\left(-\varepsilon_n \sum_{i\in I, j\in J} x_i x_j\right) = 1 - \exp(-\varepsilon_n X_I X_J).$$

Thus, the functional form of the connection probability is preserved exactly under homogeneous aggregation. Other choices, such as $\min\{\varepsilon_n x_i x_j, 1\}$ or $\varepsilon_n x_i x_j/(1+\varepsilon_n x_i x_j)$, have the same first-order behaviour when $\varepsilon_n x_i x_j$ is small, but they do not satisfy the above exact no-edge multiplicative identity. We therefore expect some qualitative features, such as the $\sqrt{n}$-scale of the leading modes and the appearance of power-law eigenfunctions, to be robust for a broader class of saturating link functions. However, the exact Gamma-function constants and the explicit logarithmic spiral are specific to the exponential connection probability, because they follow from the Laplace transform calculation used below.

Under an arbitrary homogeneous partition whereby the n nodes are aggregated into supernodes (each with the same number of participating nodes), the form of both $p_{ij} = f_n(x_i, x_j)$ and $\rho_\alpha(x)$ is unchanged, up to a parameter shift in the latter—reflecting the fact that the fitness of a supernode is the sum of the fitnesses of its constituent nodes[7,9]. Since $\rho(x)$ for positive α-stable variables is not known in closed-form (except for $\alpha = 1/2$), for analytical tractability we follow[9] and consider a pure Pareto(α) distribution with the same tail as an α-stable distribution:

$$\rho_\alpha(x) = \alpha x^{-1-\alpha} \quad 0<\alpha<1 \tag{2}$$

for $x \geq 1$, and $\rho_\alpha(x) = 0$ otherwise. We also consider $\varepsilon_n = n^{-1/\alpha}$ as a scaling that allows the graph to be arbitrarily large while remaining sparse, allowing precise asymptotic calculations for large n[9]. In this regime, the tail of the expected degree distribution $P(k)$ decays as k^{-2} irrespective of the value of α, the expected link density is of order $\ln n/n$, while the average local clustering coefficient remains finite[7,9]—which are all widespread properties found in real-world networks.

Realized versus expected matrix

We denote the realized adjacency matrix of the graph as $\mathbf{A}$, where A_{ij} is a Bernoulli variable: $A_{ij} = 1$ with probability p_{ij} and 0 otherwise. Note that $\mathbf{A}$ is symmetric and $A_{ii} = 0$. By construction, the expectation of $\mathbf{A}$ (conditioning on the realized weights) is the matrix $\mathbf{P} = \mathbb{E}[\mathbf{A}|\{x_i\}]$ with entries $P_{ij} = p_{ij} = f_n(x_i, x_j)$ and captures the deterministic, structural signal imposed by the weights, while the actual $\mathbf{A}$ can be seen as a noisy realization of that signal.

We use the term "annealed" for the sampling of the fitness variables. Conditional on the realized weights $\{x_i\}$, however, the edge variables are independent Bernoulli variables and the expected matrix is $\mathbf{P} = \mathbb{E}[\mathbf{A}|\{x_i\}]$. Thus, the spectral comparison between $\mathbf{A}$, $\mathbf{P}$, and $\mathbf{H} = \mathbf{A}-\mathbf{P}$ is naturally quenched with respect to the edge randomness. If the random weights are replaced by a deterministic sequence with the same regularly varying order statistics, for instance $x_i = (n/i)^{1/\alpha}$ after ordering, the leading asymptotic predictions remain the same, while sample-to-sample fluctuations of the outlier locations are suppressed. This is also illustrated in Fig. 2, where the deterministic and sampled Pareto weights display the same $\sqrt{n}$ scaling.

Indeed, a central idea in our analysis is to decompose the adjacency matrix into the sum of an expected component and a fluctuation component, and then use random matrix theory (RMT) intuition to separate the spectrum into bulk and outlier components. Let us write:

$$\mathbf{A} = \langle \mathbf{A} \rangle + (\mathbf{A} - \langle \mathbf{A} \rangle) = \mathbf{P} + \mathbf{H}, \tag{3}$$

where $\mathbf{H} = \mathbf{A}-\mathbf{P}$ is the zero-mean noise matrix. By construction, $\mathbf{P}$ is a dense matrix (encoding for the structure of the network) with a highly skewed pattern due to the heavy-tailed x_i, whereas $\mathbf{H}$ captures the randomness of edge realizations. If the matrix $\mathbf{P}$ were of small, finite rank and $\mathbf{H}$ were a 'typical' random matrix with a bounded spectral distribution, then standard results show that each eigenvalue of $\mathbf{P}$ above a certain magnitude would detach from the continuous spectrum of $\mathbf{H}$. This phenomenon, rigorously characterized in spiked random matrix theory, underlies applications like spectral clustering[27–29]. In our case, $\mathbf{P}$ is not finite-rank: as we show in Supplementary Information (SI), we find evidence of an 'effective' rank of order $\ln n$. Classical BBP-type results concern fixed finite-rank perturbations of random matrices. Our matrix $\mathbf{P}$ is not finite-rank, but its eigenvalues decay rapidly enough that only a slowly growing number of modes remains visible above the noise level. This places the MSM closer to recent work on growing-rank or mesoscopic perturbations, where the rank of the deterministic component may increase with n while remaining $o(n)$ [30,31]. We do not use these results directly, since our noise matrix has a heavy-tailed variance profile. The comparison is meant only to emphasize that the relevant perturbation is not finite-rank, but has an effective rank that grows sublinearly with n. An illustration of the typical spectra of $\mathbf{A}$ and $\mathbf{P}$ is provided in Fig. 1. Our main goal is the characterization of these spectra and the associated eigenvectors, with a specific attention to the outlier modes carrying structural information.

Integral eigenvalue equation. We are interested in the solution of the eigenmode equation[15]

$$\mathbf{P}v_k = \lambda_k v_k \quad k = 1,n \tag{4}$$

with $|\lambda_1| \geq |\lambda_2| \geq \cdots \geq |\lambda_n|$. Denoting the ith entry of each eigenvector v_k as $v_k^{(i)}$, we can rewrite Eq. (4) as

$$\sum_{j=1}^{n} p_{ij} v_k^{(j)} = \lambda_k v_k^{(i)} \quad i = 1,n \quad k = 1,n \tag{5}$$

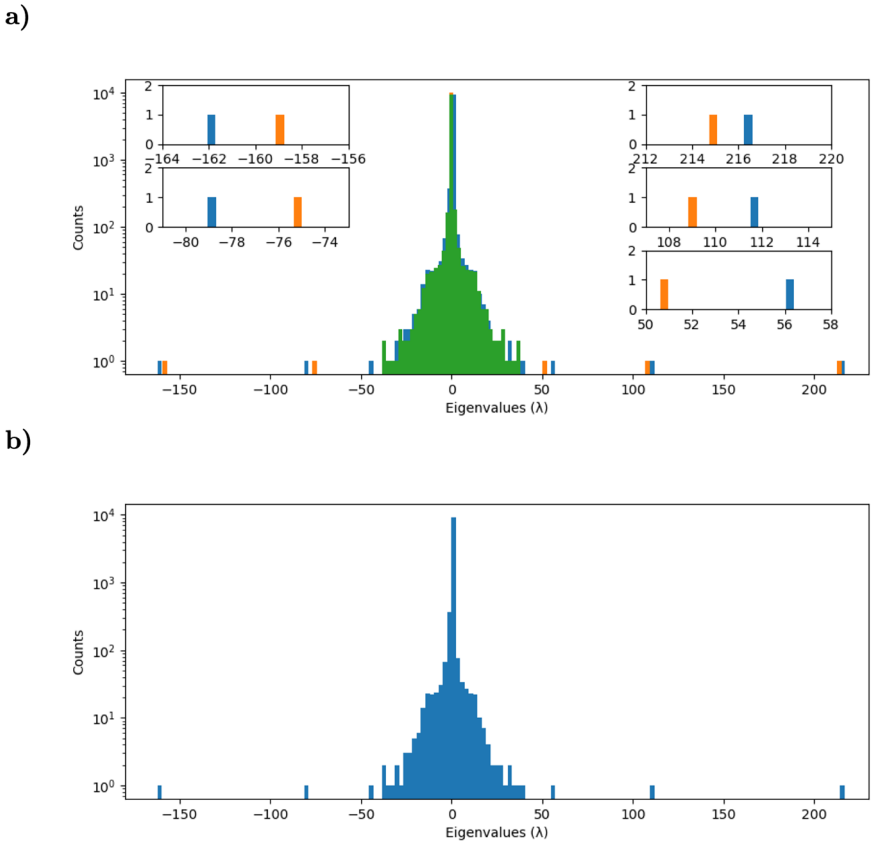

Fig. 1 | Full eigenvalue spectrum of the adjacency matrix A and its decomposition into outlier and bulk components for $n = 10^4$ and $\alpha = 0.5$. a Histogram (blue) of the eigenvalues of **A**. We see separation into atomic delta densities and a central, continuous bulk. **b** Separation of the spectrum into two regimes, the outliers being those of **A** in blue, and of **P** in orange. We also superimpose in green the eigenvalue histogram of **H**, which replicates the bulk behaviour of **A**.

Note that, since **P** is real and symmetric, its eigenvalues are real. Also note that any two vertices i, j with the same realized weight $x_i = x_j$ are statistically equivalent, as their (expected) properties in the graph depend only on the weight x. Similarly, if $x_i = x_j$ then the ith and jth entries of each eigenvector v_k will be equal: $v_k^{(i)} = v_k^{(j)}$. This allows us to write $v_k^{(i)} = v_k(x_i)$ where $v_k(x)$ must be a continuous function of the weight x. For large enough n, Eq. (5) can be recast as the integral expression

$$\mathbf{\Pi}_{\alpha,n}[v_k(x)] = \frac{\lambda_k}{n}\, v_k(x). \tag{6}$$

where $v_k(x)$ is an eigenfunction (with eigenvalue λ_k/n) of the integral operator

$$\mathbf{\Pi}_{\alpha,n}[g(x)] \equiv \int_0^{+\infty} dy\, \rho_\alpha(y)\,(1 - e^{-\varepsilon_n xy})\, g(y), \tag{7}$$

corresponding to the eigenvector v_k (with eigenvalue λ_k) of the original matrix **P**. A natural normalization for $v_k(x)$ will emerge from the calculations that follow. If an eigenfunction $v_k(x)$ is found, a convenient way to go back to the actual eigenvector entry $v_k^{(j)}$ is the following. We first order all vertices so that $x_1 \le x_2 \le \cdots \le x_n$. Then, since a pure Pareto(α) variable can be represented as a uniform random variable, raised to the power $-1/\alpha$, in the interval [0, 1], we arrive at the relation $x_j = (n/j)^{1/\alpha}$ (we will use this relation as an alternative, deterministic assignment of the fitness of nodes to produce a 'noise-free' power law distribution even for finite n). Finally,

$$v_k^{(j)} = v_k(x_j) = v_k\left(\frac{n^{1/\alpha}}{j^{1/\alpha}}\right) \quad j = 1, n \quad k = 1, n. \tag{8}$$

Largest eigenvalue and principal eigenvector

We start with the principal component $k = 1$. From the Perron–Frobenius theorem, λ_1 is positive and v_1 has all entries of the same sign. We will set the normalization of v_1 in such a way that all its entries are positive, so that $v_1(x)$ is a positive-valued function. When evaluating the operator in Eq. (7) on the eigenfunction, the multiplication of $\rho_\alpha(x)$ by $v_1(x)$ formally generates a modified, effective distribution of the weights. We then look for an eigenfunction such that $v_1(x)\rho_\alpha(x) = \rho_\beta(x)$ is again a Pareto pdf with a new index β. This is obtained for the eigenfunction

$$v_1(x) = \frac{\beta}{\alpha}\, x^{\alpha-\beta}, \quad \beta \in \mathbb{R}^+. \tag{9}$$

Setting $g(x) = v_1(x)$ into Eq. (7), we get

$$\mathbf{\Pi}_{\alpha,n}[v_1(x)] = 1 - \varphi_\beta(\varepsilon_n x) \tag{10}$$

where we have introduced the Laplace transform (LT) φ_α of the Pareto-α density, defined as

$$\varphi_\alpha(t) \equiv \int_0^{+\infty} \mathrm{d}x\, \rho_\alpha(x)\, e^{-tx} = \alpha \int_1^{+\infty} \mathrm{d}x\, x^{-1-\alpha}\, e^{-tx}, \tag{11}$$

and we have exploited the normalization property

$$\int_0^{+\infty} \mathrm{d}y\, \rho_\alpha(y)\, v_1(y) = \int_0^{+\infty} \mathrm{d}y\, \rho_\beta(y) = 1. \tag{12}$$

The above expression sets our normalization for $v_1(x)$, which is the analogue of the ℓ_1 norm $\sum_{i=1}^{n} |v_1^{(i)}| = 1$ for the original eigenvector v_1. An important asymptotic property of $\varphi_\beta(t)$ (see SI) is that, for $0 \le \beta \le 1$,

$$1 - \varphi_\beta(t) \sim t^\beta\, \Gamma(1-\beta), \qquad t \to 0^+. \tag{13}$$

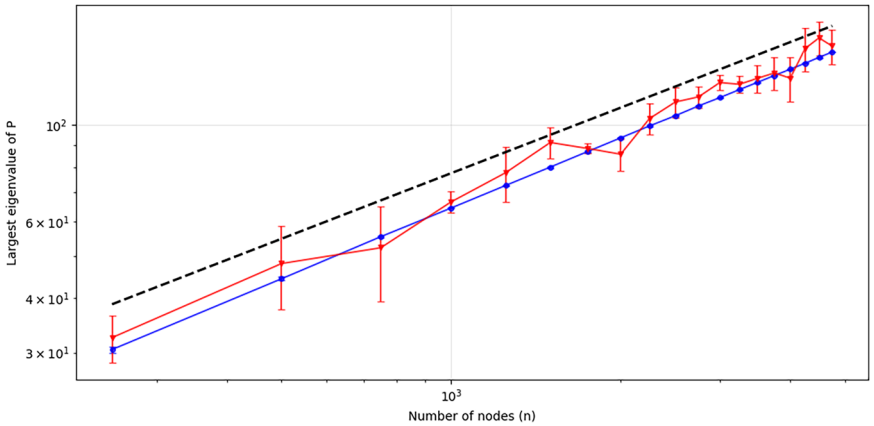

Fig. 2 | Scaling of the largest eigenvalue λ_1 of P with the number of nodes n for $\alpha = 0.5$. The largest eigenvalue λ_1 is shown as a function of n for tail index α, using two assignments of the node weights $\{x_i\}_{i=1}^n$: weights sampled independently and identically distributed from a Pareto distribution (red circles, averaged over 5 independent samples) and weights assigned deterministically as $x_i = (n/i)^{1/\alpha}$ (blue circles). Both are compared with the analytic prediction of Eq. (15) (black solid line). The close agreement across both weight assignments confirms the $\sqrt{n}$ scaling.

This allows us to confirm that $v_1(x)$ is asymptotically an eigenfunction, for a suitable choice of β. Indeed, applying Eq. (13) into Eq. (10), we can recast Eq. (6) as

$$\mathbf{\Pi}_{\alpha,n}[v_1(x)] \sim (\varepsilon_n x)^\beta \, \Gamma(1-\beta) = \frac{\lambda_1}{n}\frac{\beta}{\alpha}\, x^{\alpha-\beta} \tag{14}$$

(provided we identify $\beta \equiv \alpha - \beta$, i.e. $\beta = \alpha/2$) to find

$$\lambda_1 = \frac{\alpha}{\beta}\,\Gamma(1-\beta)\, n\, \varepsilon_n^\beta = -\alpha\,\Gamma\left(-\frac{\alpha}{2}\right) n^{1/2}. \tag{15}$$

This square-root growth of λ_1 can be confirmed via actual computations on the matrix **P** itself (see Fig. 2). Using Eq. (8), we also obtain all the eigenvector entries as

$$v_1^{(j)} = v_1(x_j) = \frac{1}{2}x_j^{\alpha/2} = \frac{1}{2}\left(\frac{n}{j}\right)^{1/2} \qquad j = 1, n. \tag{16}$$

This is also confirmed numerically later on.

Next eigenvalues

We now turn $k > 1$. Let us preliminarily introduce auxiliary complex-valued test functions $v_k^\pm(x)$ of the form still given by Eq. (9), where the role of the exponent β is now taken by its complex counterparts $\beta_k^\pm \in \mathbb{C}$:

$$v_k^\pm(x) = \frac{\beta_k^\pm}{\alpha}\, x^{\alpha-\beta_k^\pm}, \quad \beta_k^\pm \equiv \gamma_k \pm \mathbf{i}\,\omega_k \in \mathbb{C} \tag{17}$$

where $\gamma_k = \Re[\beta_k^\pm] \in \mathbb{R}$ and $\pm\omega_k = \Im[\beta_k^\pm] \in \mathbb{R}$ are the real and imaginary parts of $\beta_k^\pm$, respectively. Note that β_k^+ and β_k^- are complex conjugate. Just like $\rho_\beta(x) \equiv v_1(x)\rho_\alpha(x)$ is a Pareto pdf with modified (real) index β, which has the same tail behaviour of a stable distribution with index β, $\rho_{\beta_k^\pm}(x) \equiv v_k^\pm(x)\rho_\alpha(x)$ is formally a generalized Pareto distribution with the same 'tail behaviour' as the recently defined stable distributions with complex-valued index $\beta_k^\pm$ [32,33]. As we now show, these complex-valued scaling exponents generate log-periodicity, as typically found in systems with discrete scale invariance[14]. Indeed, in SI we derive the following expression for the eigenfunctions $v_k(x)$ for $k \geq 1$:

$$v_k(x) = \frac{1}{2}\left[\Gamma(1-\beta_k^-)\, v_k^+(x) + \Gamma(1-\beta_k^+)\, v_k^-(x)\right] \tag{18}$$

with $\gamma_k = \alpha/2$ (for all k) and associated eigenvalues

$$\lambda_k = (-1)^k\,\alpha\left|\Gamma\left(-\frac{\alpha}{2} + \mathbf{i}\,\omega_k\right)\right| n^{1/2}, \tag{19}$$

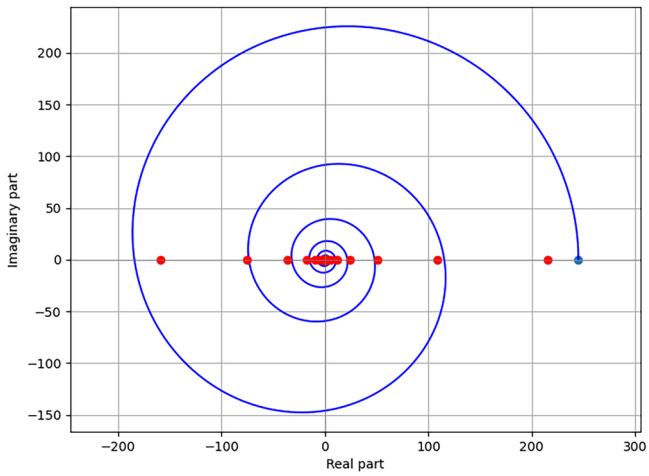

Fig. 3 | Eigenvalues of the expected adjacency matrix P lie at the intersections of the real axis with a logarithmic *spira mirabilis* in the complex plane. The actual real-valued outlier eigenvalues of **P** (red dots) are shown together with the logarithmic spiral $\sigma^+(\omega)$ (blue curve) defined in Eq. (21), plotted parametrically in the complex plane as a function of $\omega \geq 0$. Parameters: $n = 10^4$, $\alpha = 0.5$.

where the values of ω_k are defined implicitly via

$$\arg\left[\Gamma\left(-\frac{\alpha}{2} + \mathbf{i}\,\omega_k\right)\right] = \frac{\omega_k}{\alpha}\ln n - k\pi, \quad k \in \mathbb{N}_0. \tag{20}$$

Note that $k = 1$ and $\omega_1 = 0$ is a solution, coinciding with what we have already found in Eqs. (9) and (15) for the principal eigenmode. Graphically, λ_1 and all the other eigenvalues λ_k ($k > 1$) correspond to the intersections between the real axis and the two logarithmic spirals

$$\sigma^\pm(\omega) \equiv -\alpha\,\Gamma\left(-\frac{\alpha}{2} \mp i\omega\right) n^{1/2} \exp\left(\pm\,\mathbf{i}\,\frac{\omega}{\alpha}\ln n\right). \tag{21}$$

defined parametrically in the complex plane for any real value $\omega \geq 0$ (see SI). In particular, plotting $\Im[\sigma^\pm(w)]$ versus $\Re[\sigma^\pm(w)]$ generates two spirals, both starting at $\lambda_1 > 0$ for $\omega = 0$ and then shrinking clockwise (σ^-) and counterclockwise (σ^+) for $\omega > 0$, crossing the real line at the next eigenvalues λ_2, λ_3, … which alternate in sign. The admissible values ω_k defined by Eq. (20) are precisely those realizing the intersections. A comparison between these intersections (for σ^+) and the actual eigenvalues computed directly on **P** for given n and α is illustrated in Fig. 3 and in SI. Unfortunately, calculating the exact values ω_k defined by the non-invertible Eq. (20) is not possible for $k > 1$. However, in SI we derive the following approximate expression (valid for

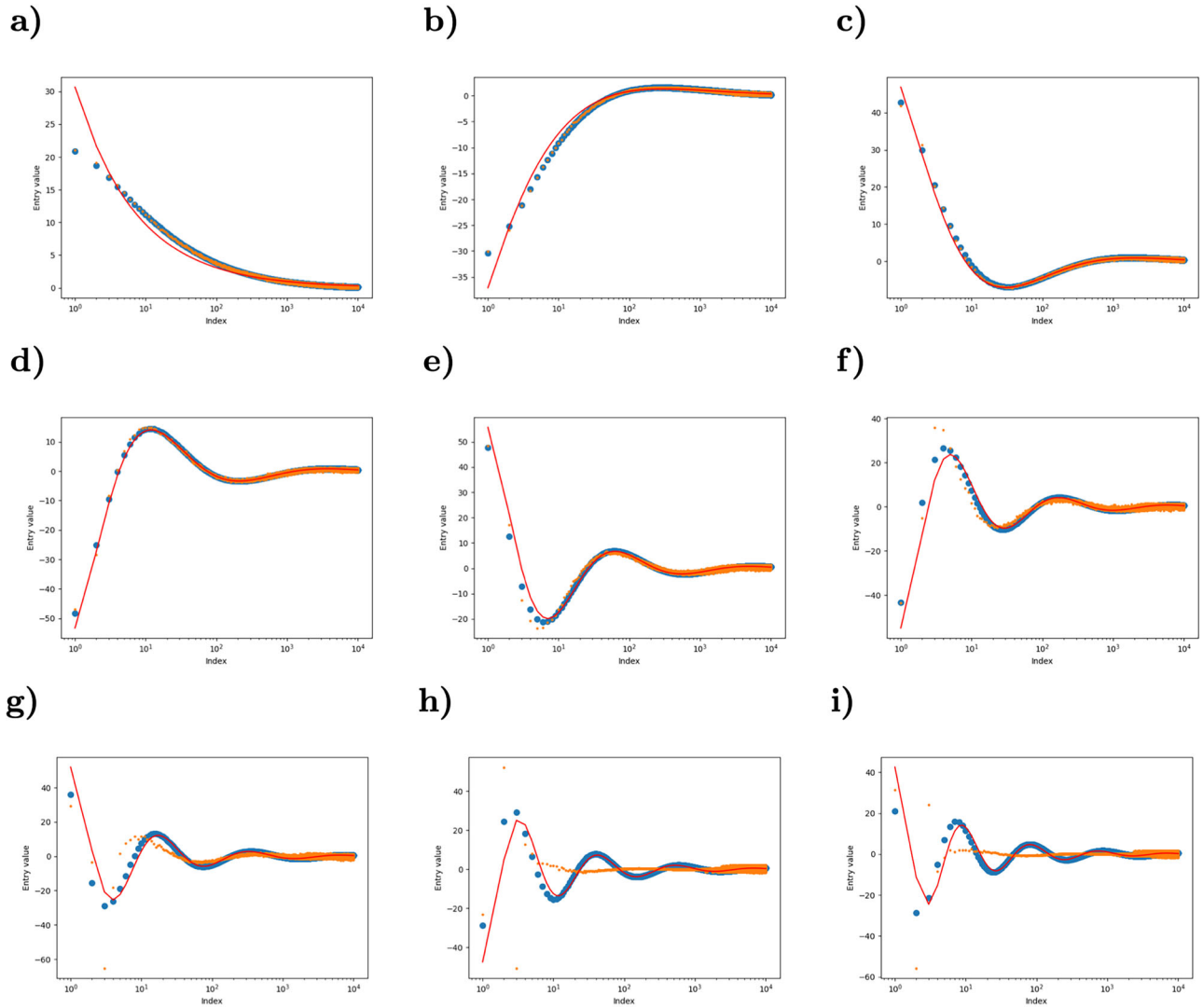

Fig. 4 | Plot of eigenvector entries $v_k(j)$ versus j for $n = 10^4$ and $\alpha = 0.5$. a First eigenvector. **b** Second eigenvector. **c** Third eigenvector. **d** Fourth eigenvector. **e** Fifth eigenvector. **f** Sixth eigenvector. **g** Seventh eigenvector. **h** Eight eigenvector. **i** Ninth eigenvector. Blue dots correspond to the actual eigenvectors entries of **P**, while red solid lines represent the corresponding predicted entries from Eq. (24). Orange dots are the entries of the eigenvectors of **A**, and we can see that in the outlier regime, they are well predicted by **P** and hence the ones we obtained analytically. We also notice a breakpoint in k after which the eigenvalues of **A** are no longer described by those of **P**, which are still predicted by Eq. (24). The agreement between the eigenvectors of **A** and those of **P** starts to deteriorate around the seventh mode in this example. In the SI, we display the companion figures for other values of α, showing that the breakpoint is changing as well when the tail index is different. This is a consequence of what we show in Fig. 5, i.e. the threshold to use to discriminate between the structural modes and those coming from randomness is a function of the tail index α.

$1 < k \lesssim \ln n$):

$$\omega_k \approx \alpha \frac{k\pi + \phi_\alpha}{\ln n}, \quad \phi_\alpha \equiv \arg\Gamma[-\alpha/2 + \mathbf{i}\,\omega_\alpha] \tag{22}$$

where $\omega_\alpha \equiv \sqrt{\frac{\alpha}{2}\left(\frac{1}{\gamma} - \frac{\alpha}{2}\right)}$ ($\gamma \approx 0.5772$ being the Euler–Mascheroni constant). Equation (22) will prove useful to determine how fast $|\lambda_k|$ decays as k grows.

Next eigenvectors

We now turn to the eigenvectors for $k > 1$. Plugging ω_k into Eq. (18), we get

$$v_k(x) = \frac{x^{\alpha/2}}{\alpha} \Re\left[\left(\frac{\alpha}{2} - \mathbf{i}\,\omega_k\right)\Gamma\left(1 - \frac{\alpha}{2} - \mathbf{i}\,\omega_k\right) x^{\mathbf{i}\omega_k}\right]. \tag{23}$$

Using Eq. (8), we re-express the eigenvector entries as

$$v_k^{(j)} = \sqrt{\frac{n}{j\alpha^2}} \Re\left[\left(\frac{\alpha}{2} - \mathbf{i}\,\omega_k\right)\Gamma\left(1 - \frac{\alpha}{2} - \mathbf{i}\,\omega_k\right)\left(\frac{n}{j}\right)^{\frac{\mathbf{i}\omega_k}{\alpha}}\right]. \tag{24}$$

Since $x^{\mathbf{i}\omega_k} = \mathrm{e}^{\mathbf{i}\omega_k \ln x}$ and $j^{\mathbf{i}\omega_k/\alpha} = \mathrm{e}^{\mathbf{i}(\omega_k/\alpha)\ln j}$, the structure of the above eigenfunctions and eigenvectors is oscillating, log-periodic in their arguments (x and j, respectively), and modulated by a power-law profile ($x^{\alpha/2}$ and $j^{-1/2}$, respectively). In Fig. 4 and in SI, we show that our analytically derived log-periodic formula tracks the actual eigenvectors of both **P** and **A** remarkably well for small k. These eigenvectors do not display traditional delta-like localization, as they are broadly supported on a wide range of weight percentiles with the largest amplitude around the hub node ($j = 1$), followed by power-law decay $j^{-1/2}$ (see also SI). As k grows large enough (below and in SI we provide evidence that this happens for k growing with n but of order at most $\ln n$), we find a departure of the eigenvectors of **A** from those of **P**, due to the entrance of the associated eigenvalues into the random

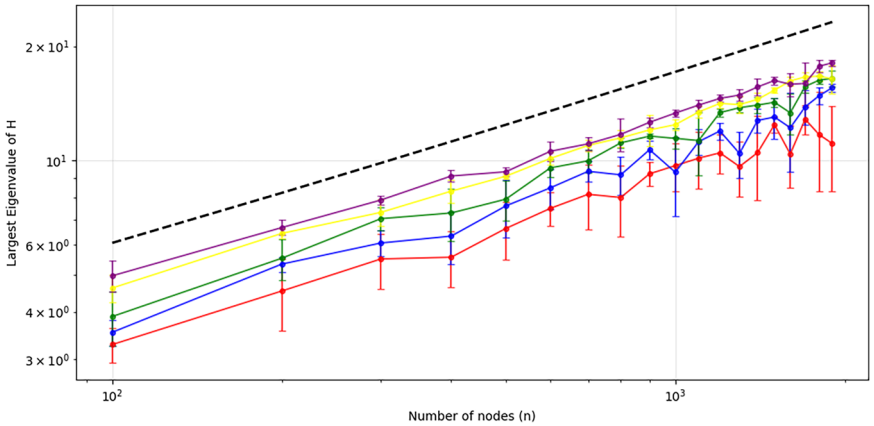

Fig. 5 | Spectral norm of the noise matrix H. The largest eigenvalue of $\mathbf{H} = \mathbf{A} - \mathbf{P}$ (i.e. the edge of the bulk), averaged over 10 independent realizations, is plotted as a function of the number of nodes n for five values of the tail index: $\alpha = 0.3$ (red circles), $\alpha = 0.4$ (blue circles), $\alpha = 0.5$ (green circles), $\alpha = 0.6$ (yellow circles), and $\alpha = 0.7$ (purple circles). The black dashed line shows the analytic upper bound $\sqrt{n}/2$ derived in Eq. (25). All curves grow as $\sqrt{n}$, and the upper bound provides a good envelope across all tested values of α, although the α-dependent prefactor requires further refinement.

bulk, where eigenvectors are expected to be more uniformly spread and less structured.

For the parameters of Fig. 4, $n = 10^4$, and hence $\ln n = \ln(10^4) \simeq 9.2$. The observed deterioration around $k \simeq 7$ is therefore compatible with a cutoff of the form

$$k_{\text{out}}(n, \alpha) \simeq c(\alpha) \ln n,$$

with a prefactor $c(\alpha) < 1$. More explicitly, if the edge of the bulk generated by $\mathbf{H}$ is $C_H(\alpha)\sqrt{n}$, then the last visible outlier is estimated by

$$k_{\text{out}}(n, \alpha) = \max\left\{k : \alpha \left|\Gamma\left(-\frac{\alpha}{2} + i\omega_k\right)\right| > C_H(\alpha)\right\}.$$

[Since ω_k is approximately proportional to $k/\ln n$ in the range considered in Eq. (22), this comparison gives a logarithmic cutoff with an α-dependent prefactor. The companion figures in the SI for other values of α show that this breakpoint changes with the tail index, as expected from the dependence of the bulk edge on α.

Bulk of the spectrum

As we have seen in Fig. 1 for the eigenvalues and from Fig. 4 for the eigenvectors (plus more illustrations in SI), there is a value of k beyond which the spectral properties of $\mathbf{P}$ are no longer able to describe those of $\mathbf{A}$. We refer to this as the 'entrance' into the random bulk, i.e. the noisy part of the spectrum generated primarily by the fluctuation of $\mathbf{H} = \mathbf{A} - \mathbf{P}$. The analysis of this part of the spectrum is highly non-trivial and is beyond the scope of this paper. Nevertheless, in SI, we show how an analytic characterization of this region is possible using RMT methods. In particular, we show that the classical form of the Dyson self-consistency equation for the resolvent is still in place, and the usual cavity method yields the same structure as a non-standard method based on Poisson point processes and representation of stable laws, which is well-suited for our special regime of weights. What we are mainly interested in here is the estimation of where the signal 'meets' the bulk. In particular, we look for an upper bound for the spectral norm of $\mathbf{H}$, whose elements $H_{ij} = A_{ij} - P_{ij}$ are independent but not identically distributed random variables in the range $[-1, 1]$, the variance of H_{ij} being $p_{ij}(1-p_{ij})$. The study of such so-called random matrices with a variance profile, or structured random matrices, is of great interest in the mathematical ecology community, and has fostered a lively discussion in the mathematical literature[34–41]. In particular, we are interested in the bound derived in ref. 40, that can be extended to matrices with entries having different subgaussian distributions, like the centred Bernoulli of our case. In SI we show that for our case the bound for the spectral norm of $\mathbf{H}$ can be attained as

$$\| \mathbf{H} \| \lesssim \frac{\sqrt{n}}{2} + \frac{1}{4}\sqrt{\ln n} \simeq \frac{\sqrt{n}}{2}. \tag{25}$$

In Fig. 5, we show that the square root growth (that is, commonplace in Wigner matrices) seems to be the right one, and that the coefficient coming from the maximization of the row/column sum of the variance profile matrix is already a quite good envelope for all values of α. Nonetheless, this crude bound needs refinement, at least to include the dependence on α. This calls for the full characterization of the bulk spectrum, which we leave to future work. What is important for our purposes here is noticing that the edge of the bulk lives on the same scale $\sqrt{n}$ as the leading eigenvalues given by Eq. (19). Since the prefactor of $\sqrt{n}$ for those outliers decays exponentially with ω_k (and, via Eq. (22), with $k/\ln n$—see SI), we see that the bulk will necessarily 'eat out' the leading eigenvalues for some value of k of order at most $\ln n$.

Discussion

In this paper, we provided a characterization of the spectral properties of the multi-scale model (MSM) in the infinite-mean regime ($0 < \alpha < 1$), which has been recently identified as an annealed random graph model that is exactly invariant under node aggregation[7,9]. This invariance is a key concept in the field of network renormalization[5], but its connection with discrete scale invariance and the associated idea of complex scaling exponents[14,42] had not been investigated so far. We showed that the leading eigenvalues of the expected adjacency matrix $\mathbf{P}$ scale as $\sqrt{n}$ and accurately proxy the outlier eigenvalues (whose number is growing and of order at most $\ln n$) of the realized adjacency matrix $\mathbf{A}$. Remarkably, these outliers have an approximately constant spacing on a logarithmic scale of their index k and can be identified as the intersection between the real axis and a *spira mirabilis* in the complex plane, a self-similar object naturally emerging in presence of complex scaling exponents and stable laws with complex stability index[32,33]. We also derived a closed-form expression for the outlier eigenvectors, showing they are delocalized but biased toward high-weight nodes. The leading eigenvectors beyond the principal (Perron–Frobenius) one exhibit log-periodic oscillations, a feature naturally produced by discrete scale invariance[14,42,43], which is here present in the property that the same random graph model describes exactly (up to a parameter rescaling) any coarse-grained version of the original graph, where sets of nodes of the same cardinality are aggregated into supernodes[7,9]. Our results qualitatively confirm the findings of Nadakuditi et al.[23,44], while partially extending them to the regime of infinite-rank perturbations of random matrices as in more recent attempts[30,31].

The leading eigenvalues, therefore, have a direct structural interpretation: they identify the deterministic multi-scale component that survives edge randomness. Estimating them accurately is useful for detecting

discrete scale invariance, for distinguishing structural outliers from the random bulk, and potentially for inferring the tail index or renormalization parameters from spectral data. The same strategy may also be useful for other heavy-tailed inhomogeneous random graphs, where the expected adjacency matrix is not finite-rank but has a hierarchy of slowly decaying structural modes. In summary, the MSM illustrates how infinite-mean heterogeneity generates spectral phenomena far from classical paradigms. Open directions include testing the universality of the $\sqrt{n}$ scaling and log-periodicity across other networks and models. More broadly, our results provide a framework for understanding spectra in multi-scale and heavy-tailed systems, and lay the ground for future work in these fields.

Methods

Graph model and parameter choices

Numerical simulations are performed on the annealed multi-scale model (MSM) defined in the "Results" section. Each graph on n nodes is generated as follows. Node fitnesses $\{x_i\}_{i=1}^n$ are drawn independently from the Pareto(α) distribution $\rho_\alpha(x) = \alpha x^{-1-\alpha}$ for $x \geq 1$, with $0 < \alpha < 1$. The connection probability between nodes i and j is $p_{ij} = 1 - \exp(-\varepsilon_n x_i x_j)$ with $\varepsilon_n = n^{-1/\alpha}$. Each edge (i, j) for $i < j$ is then drawn independently as a Bernoulli(p_{ij}) variable, and the resulting symmetric adjacency matrix $\mathbf{A}$ is stored in sparse format. In addition to random fitness assignments, we also consider deterministic fitness assignments $x_i = (n/i)^{1/\alpha}$ (nodes ranked in decreasing order), to suppress sample-to-sample fluctuations at finite n.

Eigenvalue and eigenvector computations

The expected adjacency matrix $\mathbf{P}$ with entries $P_{ij} = p_{ij}$ is stored as a dense matrix for moderate n ($n \leq 10^4$). Leading eigenvalues and eigenvectors of both $\mathbf{A}$ and $\mathbf{P}$ are computed using standard symmetric eigensolver routines (scipy.linalg.eigh). The noise matrix $\mathbf{H} = \mathbf{A} - \mathbf{P}$ is assembled, and its spectral norm (largest eigenvalue) is computed over multiple independent realizations to estimate the bulk edge. Results shown in the figures use $n = 10^4$ and are averaged over 5–10 independent realizations as indicated in the figure captions.

Analytic predictions

The analytic eigenvalue predictions (Eq. (19)) and the logarithmic spiral (Eq. (21)) are evaluated numerically by solving the implicit equation (Eq. (20)) for ω_k using the secant root-finding algorithm applied to the argument of the Gamma function. The approximate linear formula (Eq. (22)) is used as an initial guess. Eigenvector predictions (Eq. (24)) are evaluated at the node ranks $j = 1, \ldots, n$ using the same ω_k values. All special-function evaluations (Gamma function, its argument) are performed using standard scientific computing libraries in Python.

Data availability

The datasets generated and/or analysed during the current study are not publicly available due to the fact that the numerical simulations can be easily reproduced using the model definition provided in the "Methods" section, but are available from the corresponding author on reasonable request.

Code availability

The code used to generate the numerical simulations and figures in this paper is available from the corresponding author upon reasonable request.

Received: 16 January 2026; Accepted: 6 August 2026;
Published online: 25 August 2026

References

1. Caldarelli, G., Capocci, A., De Los Rios, P. & Munoz, M. A. Scale-free networks from varying vertex intrinsic fitness. *Phys. Rev. Lett.* **89**, 258702 (2002).
2. Garlaschelli, D. & Loffredo, M. I. Fitness-dependent topological properties of the world trade web. *Phys. Rev. Lett.* **93**, 188701 (2004).
3. Van Der Hofstad, R. *Random Graphs and Complex Networks* Vol. 1 (Cambridge University Press, 2017).
4. Van Der Hofstad, R.*Random Graphs and Complex Networks* Vol. 2 (Cambridge University Press, 2024).
5. Gabrielli, A., Garlaschelli, D., Patil, S. P. & Serrano, M. Á Network renormalization. *Nat. Rev. Phys.* **7**, 1–17 (2025).
6. Catanzaro, A., Garlaschelli, D. & Patil, S. P. Renormalization of interacting random graph models. *Phys. Rev. E* **113**, 024314 (2026).
7. Garuccio, E., Lalli, M. & Garlaschelli, D. Multiscale network renormalization: scale-invariance without geometry. *Phys. Rev. Res.* **5**, 043101 (2023).
8. Lalli, M. & Garlaschelli, D. Geometry-free renormalization of directed networks: scale-invariance and reciprocity. arXiv preprint arXiv:2403.00235 (2024).
9. Avena, L., Garlaschelli, D., Hazra, R. S. & Lalli, M. Inhomogeneous random graphs with infinite-mean fitness variables. arXiv preprint arXiv:2212.08462 (2022).
10. Milocco, R., Jansen, F. & Garlaschelli, D. Multi-scale node embeddings for graph modeling and generation. arXiv preprint arXiv:2412.04354 (2024).
11. Catanzaro, A., van der Hofstad, R. & Garlaschelli, D. Clustering without geometry in sparse networks with independent edges. arXiv: 2603.13159 (2026).
12. Garcia-Perez, G., Boguna, M. & Serrano, M. A. Multiscale unfolding of real networks by geometric renormalization. *Nat. Phys.* **14**, 583–589 (2018).
13. Boguna, M. et al. Network geometry. *Nat. Rev. Phys.* **3**, 114–135 (2021).
14. Sornette, D. Discrete-scale invariance and complex dimensions. *Phys. Rep.* **297**, 239–270 (1998).
15. Van Mieghem, P. *Graph spectra for complex networks* (Cambridge University Press, Cambridge, 2023).
16. Benaych-Georges, F. & Knowles, A. Lectures on the local semicircle law for Wigner matrices. arXiv preprint arXiv:1601.04055 (2016).
17. Bai, Z. & Silverstein, J. W. *Spectral Analysis of Large Dimensional Random Matrices* Vol. 20 (Springer, 2010).
18. Farkas, I. J., Derényi, I., Barabási, A.-L. & Vicsek, T. Spectra of "real-world" graphs: beyond the semicircle law. *Phys. Rev. E* **64**, 026704 (2001).
19. Poley, L., Galla, T. & Baron, J. W. Eigenvalue spectra of finely structured random matrices. *Phys. Rev. E* **109**, 064301 (2024).
20. Baron, J. W., Jewell, T. J., Ryder, C. & Galla, T. Eigenvalues of random matrices with generalized correlations: a path integral approach. *Phys. Rev. Lett.* **128**, 120601 (2022).
21. Chung, F., Lu, L. & Vu, V. Spectra of random graphs with given expected degrees. *Proc. Natl. Acad. Sci. USA* **100**, 6313–6318 (2003).
22. Baik, J., Ben Arous, G. & Péché, S. Phase transition of the largest eigenvalue for nonnull complex sample covariance matrices. *Ann. Probab.* **33**, 1643–1697 (2005).
23. Nadakuditi, R. R. & Newman, M. E. Spectra of random graphs with arbitrary expected degrees. *Phys. Rev. E* **87**, 012803 (2013).
24. Cizeau, P. & Bouchaud, J.-P. Theory of Lévy matrices. *Phys. Rev. E* **50**, 1810–1822 (1994).
25. Benaych-Georges, F., Guionnet, A. & Male, C. Central limit theorems for linear statistics of heavy tailed random matrices. *Commun. Math. Phys.* **329**, 641–686 (2014).
26. Arous, G. B. & Guionnet, A. The spectrum of heavy tailed random matrices. *Commun. Math. Phys.* **278**, 715–751 (2008).
27. Zhang, X., Nadakuditi, R. R. & Newman, M. E. Spectra of random graphs with community structure and arbitrary degrees. *Phys. Rev. E* **89**, 042816 (2014).
28. Krzakala, F. et al. Spectral redemption in clustering sparse networks. *Proc. Natl. Acad. Sci. USA* **110**, 20935–20940 (2013).
29. Bordenave, C., Lelarge, M. & Massoulié, L. Non-backtracking spectrum of random graphs: community detection and non-regular

Ramanujan graphs. In *2015 IEEE 56th Annual Symposium on Foundations of Computer Science* 1347–1357 (IEEE, 2015).
30. Afanasiev, I., Berlyand, L. & Kiyashko, M. Asymptotic behavior of eigenvalues of large rank perturbations of large random matrices. arXiv preprint arXiv:2507.12182 (2025).
31. Huang, J. Mesoscopic perturbations of large random matrices. *Random Matrices: Theory Appl.* **7**, 1850004 (2018).
32. Alexeev, I. Stable random variables with complex stability index, i. *Theory Probab. Its Appl.* **67**, 335–351 (2022).
33. Alexeev, I. Stable random variables with complex stability index, ii. *Theory Probab. Its Appl.* **67**, 499–515 (2023).
34. Van Handel, R. On the spectral norm of Gaussian random matrices. *Trans. Am. Math. Soc.* **369**, 8161–8178 (2017).
35. Latała, R. Some estimates of norms of random matrices. *Proc. Am. Math. Soc.* **133**, 1273–1282 (2005).
36. Riemer, S. & Schütt, C. On the expectation of the norm of random matrices with non-identically distributed entries. *Electron. J. Probab.* **18**, 1–13 (2013).
37. Cheliotis, D. & Louvaris, M. The limit of the operator norm for random matrices with a variance profile. *Electron. J. Probab.* **30**, 1–33 (2025).
38. Benaych-Georges, F., Bordenave, C. & Knowles, A. Spectral radii of sparse random matrices. In *Annales de l'Institut Henri Poincaré–Probabilités et Statistiques* Vol. 56, 2141–2161 (Institut Henri Poincaré, 2020).
39. Benaych-Georges, F., Bordenave, C. & Knowles, A. Largest eigenvalues of sparse inhomogeneous Erdős–Rényi graphs. *Ann. Probab.* **47**, 1653–1676 (2019).
40. Bandeira, A. & van Handel, R. Sharp nonasymptotic bounds on the norm of random matrices with independent entries. *Ann. Probab.* **44**, 2479–2506 (2016).
41. Van Handel, R. Structured random matrices. In *Convexity and Concentration* 107–156 (2017).
42. McWhirter, J. & Pike, E. R. On the numerical inversion of the Laplace transform and similar Fredholm integral equations of the first kind. *J. Phys. A: Math. Gen.* **11**, 1729–1745 (1978).
43. Ostrowsky, N., Sornette, D., Parker, P. & Pike, E. Exponential sampling method for light scattering polydispersity analysis. *Opt. Acta: Int. J. Opt.* **28**, 1059–1070 (1981).
44. Benaych-Georges, F. & Nadakuditi, R. R. The eigenvalues and eigenvectors of finite, low rank perturbations of large random matrices. *Adv. Math.* **227**, 494–521 (2011).

Acknowledgements

This publication is part of the project ``Redefining renormalization for complex networks'' with file number OCENW.M.24.039 of the research programme Open Competition Domain Science Package 24-1, which is (partly) financed by the Dutch Research Council (NWO) under the grant https://doi.org/10.61686/PBSEC42210.This work is also supported by the European Union—NextGenerationEU and funded by the Italian Ministry of University and Research (MUR)—National Recovery and Resilience Plan (Piano Nazionale di Ripresa e Resilienza, PNRR), projects "Strengthening the Italian RI for Social Mining and Big Data Analytics'' (SoBigData.it, grant IR0000013, DN. 3264, 28/12/2021), "Reconstruction, Resilience and Recovery of Socio-Economic Networks'' (RECON-NET, EP_FAIR_005-PE0000013 "FAIR''—PNRR M4C2 Investment 1.3), "A Multiscale integrated approach to the study of the nervous system in health and disease'' (MNESYS, PE0000006, DN. 1553, 11/10/2022).

Author contributions

A.C., R.S.H. and D.G. conceived and performed the analytical derivations and prepared the manuscript. A.C. conducted the numerical simulations, R.S.H. contributed to the mathematical framework, D.G. supervised the project and critically revised the manuscript. All authors read and approved the final manuscript.

Competing interests

The authors declare no competing interests.

Additional information

Supplementary information The online version contains supplementary material available at https://doi.org/10.1038/s44260-026-00098-8.

Correspondence and requests for materials should be addressed to Alessio Catanzaro.

Reprints and permissions information is available at http://www.nature.com/reprints

Publisher's note Springer Nature remains neutral with regard to jurisdictional claims in published maps and institutional affiliations.

Open Access This article is licensed under a Creative Commons Attribution 4.0 International License, which permits use, sharing, adaptation, distribution and reproduction in any medium or format, as long as you give appropriate credit to the original author(s) and the source, provide a link to the Creative Commons licence, and indicate if changes were made. The images or other third party material in this article are included in the article's Creative Commons licence, unless indicated otherwise in a credit line to the material. If material is not included in the article's Creative Commons licence and your intended use is not permitted by statutory regulation or exceeds the permitted use, you will need to obtain permission directly from the copyright holder. To view a copy of this licence, visit http://creativecommons.org/licenses/by/4.0/.

© The Author(s) 2026

This Article in Press is shared early to give you faster access to new research. It is citable and carries a permanent DOI. The final edited version will replace it automatically.